

DEPARTMENT OF MATHEMATICAL SCIENCES
COLLEGE OF SCIENCES
OLD DOMINION UNIVERSITY
NORFOLK, VIRGINIA 23529

IN-76-CR
37970
P-48

**MODELING Cr-to-Tm AND Cr-to-Tm-to-Ho
ENERGY TRANSFER IN YAG CRYSTALS**

By

John Swetits, Principal Investigator

Final Report
For the period ended November 30, 1989

Prepared for
National Aeronautics and Space Administration
Langley Research Center
Hampton, Virginia 23665

Under
Research Grant NAG-1-957
Mr. Philip Brockman, Technical Monitor
FED-Laser Technology & Applications Branch

(NASA-CR-187764) MODELING Cr-TO-Tm AND
Cr-TU-Tm-TU-Ho ENERGY TRANSFER IN YAG
CRYSTALS Final Report, period ending 30 Nov.
1989 (Old Dominion Univ.) 48 p CSCL 20L

N91-30962

Unclas
G3/76 0037970

September 1991

DEPARTMENT OF MATHEMATICAL SCIENCES
COLLEGE OF SCIENCES
OLD DOMINION UNIVERSITY
NORFOLK, VIRGINIA 23529

**MODELING Cr-to-Tm AND Cr-to-Tm-to-Ho
ENERGY TRANSFER IN YAG CRYSTALS**

By

John Swetits, Principal Investigator

Final Report
For the period ended November 30, 1989

Prepared for
National Aeronautics and Space Administration
Langley Research Center
Hampton, Virginia 23665

Under
Research Grant NAG-1-957
Mr. Philip Brockman, Technical Monitor
FED-Laser Technology & Applications Branch

Submitted by the
Old Dominion University Research Foundation
P.O. Box 6369
Norfolk, Virginia 23508-0369



September 1991

ACKNOWLEDGMENTS

The attached reprint entitled, "Energy Transfer in Cr, Tm:YAG," Advances in Nonradiative Processes in Solids, Edited by B. Di Bartolo, Plenum Press, N.Y., 1991 and preprint entitled, "Temporal Model of an Optically Pumped Co-Doped Solid State Laser" are being submitted in lieu of a final report for NAG-1-957.

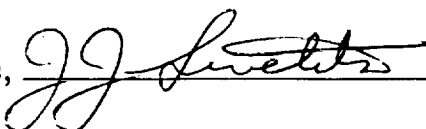
OLD DOMINION UNIVERSITY

Norfolk, Virginia 23529
804-683-3000

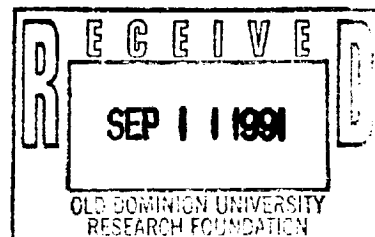
To: Mr. Bob Wolfson, Executive Director

Old Dominion University Research Found.

From: J.J. Swetits,



Professor, Department of Mathematics an



Date: September 9, 1991

Subj: Final Report for N.A.S.A. Grant NAG-1-957

The research conducted under this grant focused on two areas. The first area was energy transfer from C_r to T_m and from C_r to T_m to H_0 in YAG crystals. The primary aim was to test the model of donor luminescence of Inokuti and Hirayama (J. Chemical Physics, 43 (1965), p. 1978-1989) and the model of acceptor luminescence of Ostroumov, Privis, Smirnov and Shcherbakov (J. Opt. Soc. Am. B, 3 (1986), p. 81 - 93). Some of the results are reported in the attached reprint, "Energy Transfer in C_r, T_m : YAG."

The second area that was investigated was a mathematical model of a solid state laser in which holmium is sensitized with thulium. The results of this effort formed the basis of the doctoral dissertation of my student, T.G. Wangler. The principal results are summarized in the attached preprint, "Temporal Model of an Optically Pumped Co-Doped Solid State Laser." The paper has been submitted to the journal, Mathematical and Computer Modeling.

Acknowledgement of grant support appears on the final page of each paper.

ENERGY TRANSFER IN Cr,Tm:YAG

A.M. Buoncristiani and G. Armagan
Christopher Newport College
Newport News, VA 23606 USA

B. Di Bartolo
Boston College
Chestnut Hill, MA 02167 USA

J.J. Swetits
Old Dominion University
Norfolk, VA 23508 USA

ABSTRACT

We describe a systematic analysis of energy transfer processes in crystals of YAG doped with varying concentrations of Cr and Tm. We use both spectral measurements and measurements of the temporal response to pulsed excitation to give independent determinations of the microscopic interaction parameter for Cr to Tm transfer. We discuss the different factors in influencing the temperature dependence of the Cr to Tm transfer. Finally, we determine the dependence of the Tm cross-relaxation rate on Tm concentration.

I. INTRODUCTION

Recently there has been an interest in the development of a solid state laser operating in the "eye-safe" region of the spectrum (wavelengths greater than 1.54 microns). This interest has led to renewed studies of the interionic processes among Cr, Tm and Ho ions in various crystalline hosts. The $^5I_7 \rightarrow ^5I_8$ transition of the triply ionized Holmium ion is a good candidate for a 2-micron laser as it has a large cross-section and a long upper state lifetime. Thulium is expected to be a good sensitizer for Holmium because it has an efficient cross relaxation and energy transfer coupling to the upper laser level of Ho. Furthermore, Thulium absorbs around 780 nm so it could be pumped directly

PRECEDING PAGE BLANK NOT FILMED

by a semiconductor diode laser or indirectly by energy transfer from flashlamp pumped Chromium. In order to obtain pulses short enough for several of the proposed applications it is necessary to operate the laser in a Q-switched mode. Design of lasers to operate in this mode requires a thorough knowledge of the transfer rates for each of the various interionic processes coupling the energy of the pump to the laser transitions. We have initiated a systematic study of the energy transfer among Cr, Tm and Ho ions in YAG as a first step in the analysis of Q-switched operation of lasers based on the Ho ion sensitized by Cr and Tm. In this paper we shall focus on the Cr, Tm system, describing a general set of procedures aimed at obtaining detailed information on the energy transfer processes. We shall also mention the cross relaxation process in Tm. This work provides a clear example of the energy transfer processes discussed in references 1 and 2.

II. CHROMIUM TO THULIUM ENERGY TRANSFER

II.A. The Transfer Process

The energy levels of Cr and Tm are shown in Figure 1. We shall be interested in the following energy pathway. Energy absorbed in the broad Cr absorption bands (4T_1 , 4T_2) rapidly goes to the 2E level. From Cr: 2E the energy transfers to the Tm 3F_2 and 3F_3 levels. From there it nonradiatively populates the 3H_4 level. Tm may undergo a cross-relaxation [3H_4 , ${}^3H_6 \rightarrow {}^3F_4$, 3F_4] to the 3F_4 level from which it feeds the upper laser level in Ho. In this article we shall focus attention on the Cr to Tm transfer and the Tm cross-relaxation.

We are considering a crystalline host in which two ionic species can carry an optical excitation; donor ions D are initially excited and may subsequently transfer this excitation to acceptor ions A. The rate of energy transfer, by a dipole-dipole transition, from a donor ion to an acceptor ion separated by a distance R is proportional to the inverse of the sixth power of R, [3]

$$W_{DA} = C^{(6)}/R^6. \quad (1)$$

The coefficient $C^{(6)}$ is called the microscopic interaction parameter. It is convenient to express it in terms of the effective decay time of the donor ion (in the absence of any acceptors) τ_0 and a characteristic interaction radius R_0

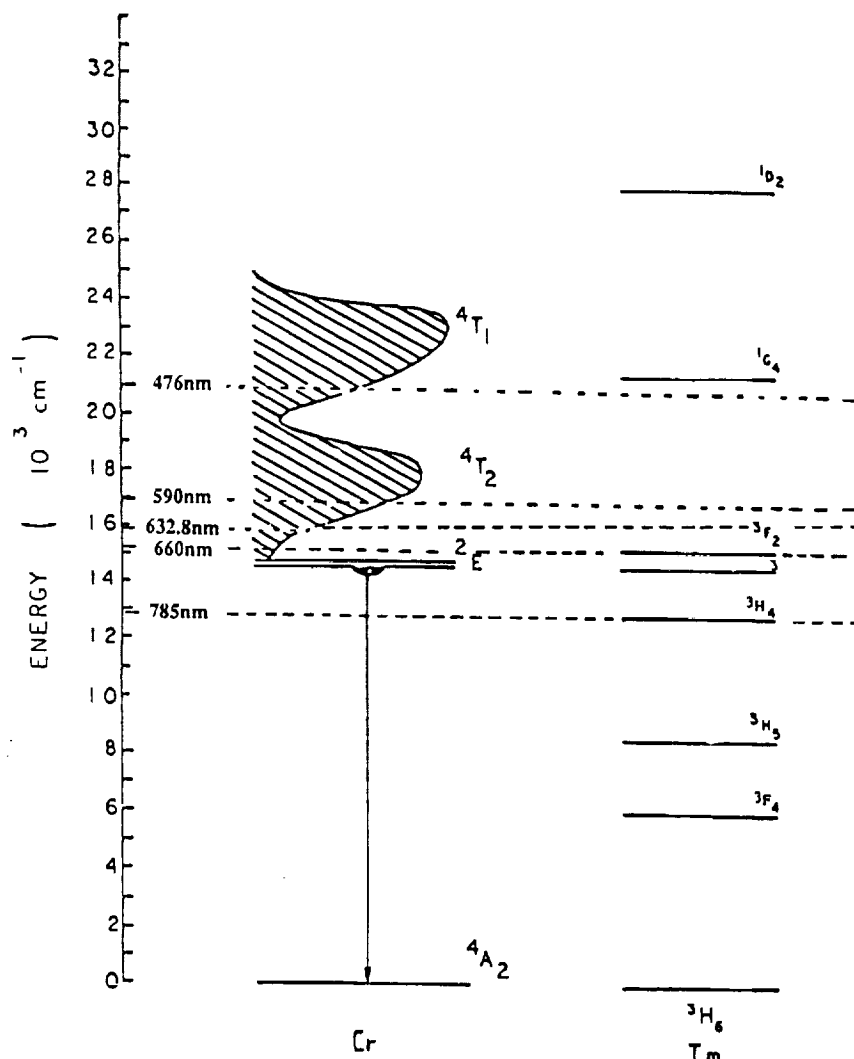


Figure 1. Energy levels of Cr, and Tm in YAG.

$$C^{(6)} = R_0^6 / \tau_0. \quad (2)$$

When the two ions are separated by R_0 the rate of energy transfer to an acceptor is equal to the decay rate for an isolated donor.

Generally speaking we are considering two types of measurements - steady state spectral measurements and measurements of the temporal response to pulsed excitation. We can use each type of measurement to get an independent determination of the inter-ionic interaction rate.

Experiments with pulsed excitation lead to effective decay times of the donor ion. This decay time in a sample without acceptors gives the lifetime of the donor level τ_0 and in a sample with acceptors it displays the lifetime shortening due to the energy transfer process. Experiments

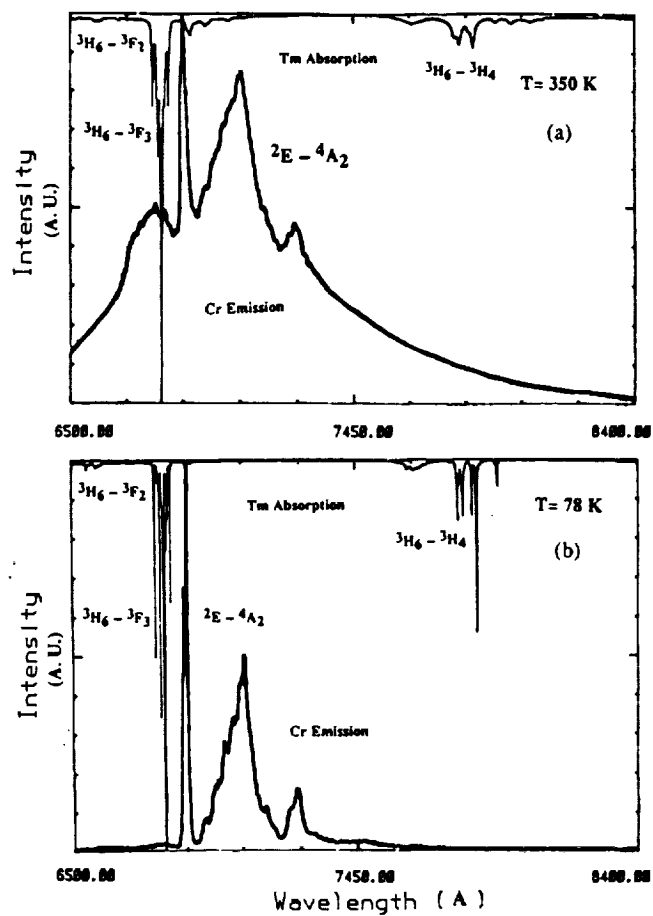


Figure 2. The Tm absorption spectrum and the Cr emission spectrum are shown for two temperatures.

with steady state excitation yield the emission spectra of the donor ions and the absorption spectra of the acceptor ion.

We should mention here that the donor ions may also transfer energy among themselves, diffusing the excitation. The more donor diffusion competes with donor to acceptor energy transfer the more difficult it is to extract information from the examination of the donor luminescence. This interference increases with increasing concentration of donors and leads to the different regimes discussed in reference 2.

II.B. Temperature Dependence of Energy Transfer

An important part of the experimental strategy demonstrated here involves examination of the variation of the various physical quantities with temperature. There are several ways in which the temperature dependence of these phenomena yield valuable information. First of all, there is some intrinsic interest in the temperature dependence of these factors. In addition, there is evidence that two phenomena may be related if they share the same temperature dependence. Finally, a statistical enhancement of the data accrues from the examination of the tendency of thermal variation.

II.C. Spectroscopic Measurements

As discussed in reference 1 there are three separate factors which contribute to the microscopic interaction parameter - the oscillator strengths for electronic dipole-dipole transitions in the donor ion emissions and in acceptor ion absorption and the spectral overlap between the donor emission and the acceptor absorption. The first of these, the donor oscillator strength, is proportional to the reciprocal of the decay time of the donor (in the absence of acceptors); this can be determined directly from the decay curves. The second, the acceptor oscillator strength is proportional to the integral of the acceptor absorption spectra over the wavelength range of the manifold. The third, the overlap integral can be calculated from the donor emission and the acceptor absorption spectra.

Figure 2 shows the Tm absorption spectrum and the Cr emission spectrum for two temperatures. While both spectra show broadening with temperatures the Cr broadening is much more extensive. There is a sideband developing on the high energy side of the Cr- Emission lines which overlaps with the ($^3H_6 \rightarrow ^3H_4$) Tm absorption. The temperature dependence of the overlap integral is due primarily to the development of

this sideband in resonance with Tm absorption. The Tm absorption does not change significantly with temperature and consequently the Tm oscillator strength remains constant with temperature. Using this spectral data we can determine the temperature dependence of the Cr-Tm overlap and the Tm absorption oscillator strength. The oscillator strength of the Cr emission is proportional to the reciprocal lifetime of Cr in the absence of Ho. The temperature dependence of each of these three factors is shown in Fig. 3. As can be seen there is little change of the Tm absorption integral with temperature over the range of temperature shown. There is a slight change in the overlap integral at lower temperatures reflecting the development of the anti-Stokes sideband. At the higher temperatures of interest in laser operation the dominant change in the microscopic interaction parameter is due to changes in the Cr emission oscillator strength.

II.D. Time Resolved Spectra

The time resolved spectra also gives evidence of the energy transfer. As can be seen in Figure 4, the temporal response to pulsed excitation for Cr alone is exponential. For crystals with higher Tm concentration this response becomes non-exponential. At early times it displays the rapid transfer of excitation from Cr to those Tm ions which are nearby. As time increases and the number of available nearby Tm ions decreases, the energy transfer rate diminishes and the decay curve settles into an exponential behavior. Evidence for energy migration among the Cr ions can be seen in the slopes of the decay curves at longer times. As the concentration of Cr increases the magnitude of the slopes increases.

As shown in (1) the time dependence of the decay curve is given by

$$I(t) = I_0 \rho(t) \quad (3)$$

where $\rho(t)$ is given explicitly in reference 1. Taking the natural logarithm of this we obtain an expression that is quadratic in $t^{1/2}$ and depends on three parameters.

$$\ln(I(t)) = \alpha - \beta t^{1/2} - \gamma t \quad (4)$$

The measured data was fit to this expression to find the values of (α, β, γ) that minimize mean square error. As shown in reference 1 these parameters are

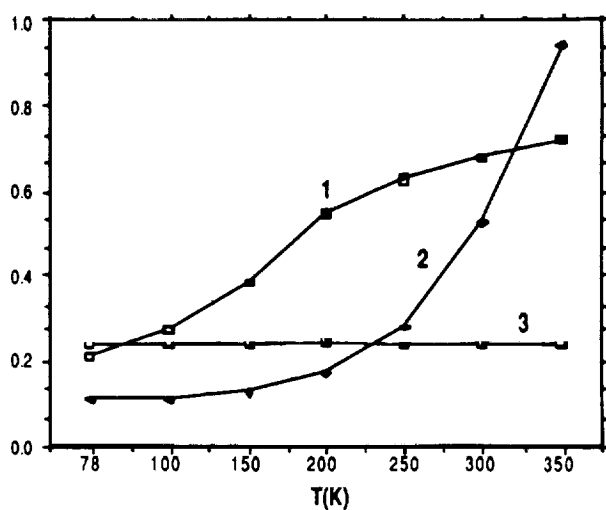


Figure 3. The time dependence of the three factors determining the microscopic interaction parameter. 1) Cr,Tm overlap integral $\times 10^{20} \text{ cm}^5$, 2) reciprocal lifetime of Cr (1/microsec), 3) Tm absorption coefficient integral $\times 10^{-3} (\text{cm}^2)$.

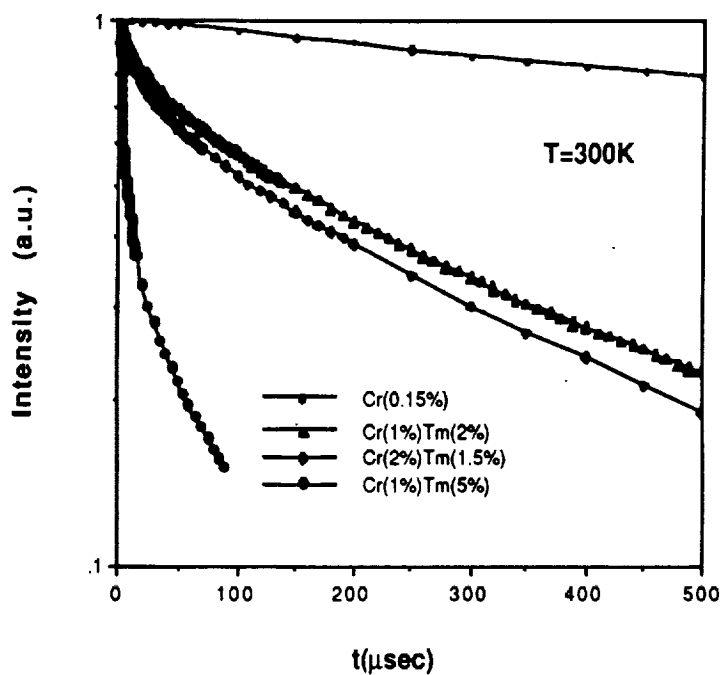


Figure 4. The temporal response to pulsed excitation for three samples of Cr and Tm doped YAG.

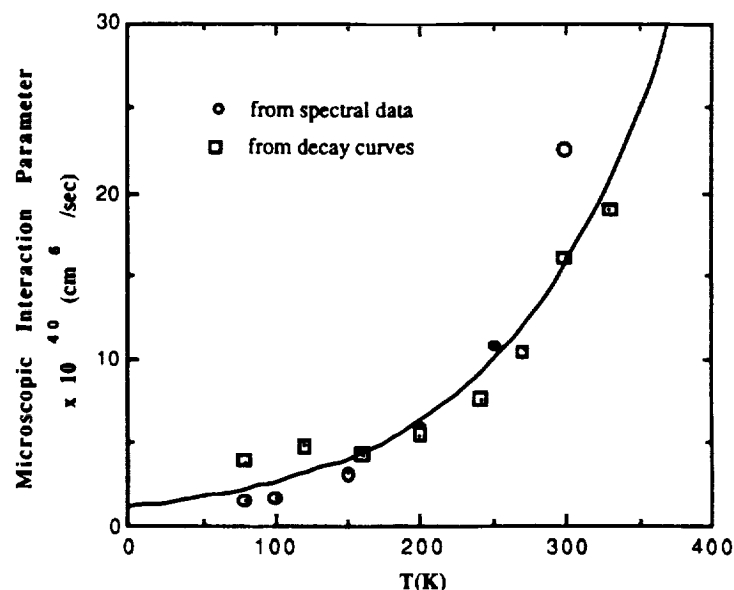


Figure 5. The microscopic interaction parameter determined by both spectroscopic measurements and by fitting the decay curves to temporal response predicted in Eq.(4).

$$\begin{aligned}
 \alpha &= \ln(I_0) \\
 \beta &= (\pi/\tau_0)^{1/2} (C/C_0) \\
 \gamma &= 1/\tau_0 + K_D
 \end{aligned}
 \tag{5}$$

After obtaining the best fitting, we compare the measured life time with the coefficient of t .

II.E. Cr to Tm Microscopic Interaction Parameter

As we have discussed, it is possible to determine the microscopic interaction parameter by two independent techniques, one using spectroscopic data and the other from time resolved data. The microscopic interaction parameter calculated from both techniques is shown in Figure 5. As evident there is qualitative agreement between the results of the two methods. The curved line shown in the figure is a best fit to the data points; as discussed previously the temperature dependence of the microscopic interaction parameter is due to the three independent factors so that the shape of the fitted curve cannot be explained further.

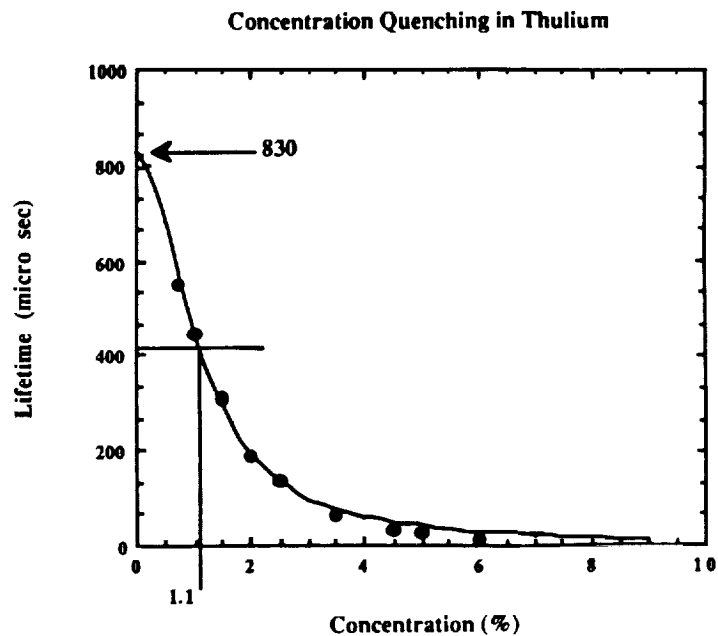


Figure 6. The lifetime of the $^3\text{H}_4$ level of Tm as a function of Tm concentration. The curve is then given by Eq.6.

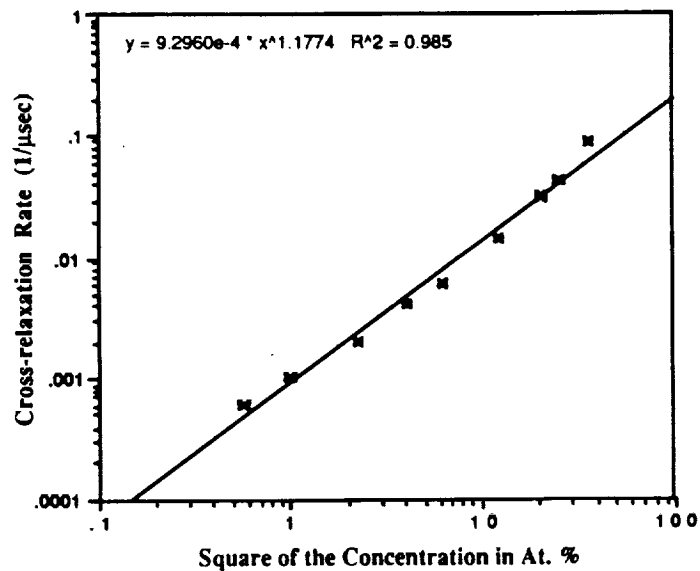


Figure 7. The rate of cross relaxation from the $^3\text{H}_4$ level of Tm as a function of the square of the Tm concentration.

III. THULIUM CROSS-RELAXATION

Finally, we wish to describe the Tm cross relaxation process. To determine the transfer rate we examine the concentration quenching of Tm. That is the decrease in lifetime of the Tm level with increasing concentration. This concentration quenching effect is shown in Figure 6. Fitting the concentration dependence of the lifetime to the quadratic formula

$$\tau = \tau_0 / [1 + (C/C_0)^2] \quad (6)$$

we can determine the intrinsic lifetime of Tm 3H_4 and the associated half concentration (the concentration of Tm at which the intrinsic lifetime is decreased by half). Using the intrinsic lifetime we can then separately determine the cross-relaxation rate. The concentration dependence of this rate is shown in Figure 7.

IV. SUMMARY

In this paper we have described an analysis of energy transfer processes occurring in Cr, Tm:YAG. We have used both spectral measurements and decay curves to provide separate determinations of the microscopic interaction parameter for the Cr to Tm transfer. By examining the temperature dependence of the various factors contributing to the microscopic interaction parameter we have been able to demonstrate that its temperature variation, above 200K, is due primarily to changes in the Cr lifetime. Concentration quenching in the Tm cross-relaxation led to a determination of the cross-relaxation rate.

This work was performed at the Solid State Laser Materials Laboratory, NASA Langley Research Center, Hampton, VA and supported by NASA grants NAG-1-796, NAG-1-955 and NAG-1-957.

REFERENCES

1. G. Armagan, B. Di Bartolo and A.M. Buoncristiani, J. of Luminescence, 44, 129 (1989).
2. G. Armagan, B. Di Bartolo and A.M. Buoncristiani, J. of Luminescence, 44, 141 (1989).
3. B. Di Bartolo, These Proceedings.

Temporal Model of an Optically Pumped Co-Doped Solid State Laser

T.G. Wangler¹

Department of Mathematics and Computer Science
Illinois Benedictine College
Lisle, Il. 60532, USA

J.J. Swetits

Department of Mathematics
Old Dominion University
Norfolk, VA. 23508, USA

A.M. Buoncristiani

National Aeronautics and Space Administration
Langley Research Center
Hampton, VA. 23665, USA

¹Will receive correspondence and proofs for correction

Abstract

Recently, research has been conducted on the optical properties of materials associated with the development of a solid-state laser in the 2 micron region. In support of this effort a mathematical model describing the energy transfer in a holmium laser sensitized with thulium is developed. In this paper we establish some qualitative properties of the solution of the model, such as nonnegativity, boundedness and integrability. A local stability analysis is then performed from which conditions for asymptotic stability are obtained. Finally, we report on our numerical analysis of the system and how it compares with experimental results.

Introduction

In the early 1980's there was a renewal of interest in solid-state lasers, due in large part to the development and availability of new host materials. It was around this time that NASA began investigating tunable solid-state lasers as promising candidates for the Earth Observing System(Eos). During the past several years research has been conducted on the sensitized holmium laser, which operates in the near infra-red region. It can be used as a source for both LIDAR(*L*ight *D*etection *A*nd *R*anging) and DIAL(*D*ifferential *A*bsorption and *L*idar) as well as on aircraft to make Doppler lidar measurements of windshear since it operates in the eye-safe region.

In a solid-state laser, a dopant ion substitutes directly into the host lattice. When the lanthanide rare earth ion holmium(Ho) is used as a dopant in the host crystal yttrium aluminum garnet($Y_3Al_5O_{12}$), the holmium ion substitutes into the yttrium sites. This induces a weak coupling to the host lattice that results in narrower absorption and emission features than those commonly observed in transition metals. Although the holmium laser has high gain and good energy storage properties, ionic interactions among the holmium ions limit the concentration of holmium possible in any host; therefore to increase the optical energy absorbed, a sensitizing ion is included. In the laser system under consideration, the lanthanide rare earth ion thulium(Tm) is used as a sensitizer for holmium. The interactions between thulium and holmium ions increase the efficiency of the Tm-Ho laser but at the cost of introducing more nonlinearities into the model.

These nonlinearities make both the analysis and the laser dynamics significantly different than solid-state laser dynamics studied previously.

The model comprises thulium ions in energy levels 3H_4 , 3F_4 , and 3H_6 ; holmium ions in energy levels 5I_5 , 5I_7 , and 5I_8 ; and the photon density in the optical cavity. There are two main types of processes considered in the laser system; namely, those processes that are inter-ionic—involving the transfer of excitation from one ion to another—and those that are not. Inter-ionic processes include: cross relaxation, back transfer, and up-conversion. Processes that are not inter-ionic include: spontaneous emission, absorption and stimulated emission. The model does not account for spatial dependence of excitation in the crystal rod but rather utilizes a spacial average over the length of the rod.

In the next section, the system of equations for the electron populations and photon density is introduced and discussed. We then establish some qualitative properties of the solution to the system. After that a local stability analysis is performed and finally the system is subjected to a numerical treatment and the numerical solution compared with experimental results obtained in the laboratory.

The Model of the Laser Dynamics

The energy level diagram for the Tm^{3+} ion and the Ho^{3+} ion in YAG [1] is the basis for the idealized model, Figure 1, of lasing action. Insert Figure 1 For the remainder of the discussion the following correspondence is made as a matter of notational convenience: thulium energy levels 3H_6 , 3F_4 , and 3H_4 correspond to energy levels 0, 1, and 2, respectively and holmium energy levels 5I_8 , 5I_7 , and

$^5\text{I}_5$ correspond to energy levels $0', 1'$, and $2'$ respectively. The number of thulium ions, per cm^3 , in energy level i and at time t will be denoted $N_i(t)$; $i = 0, 1, 2$. Similarly, the number of holmium ions, per cm^3 , in energy level i' and at time t will be denoted $n_i(t)$; $i = 0, 1, 2$.

The temporal evolution of the dopant electron populations is described by the set of rate equations given by

$$\frac{dN_2(t)}{dt} = W_p(t)N_0(t) - \frac{N_2(t)}{\tau_2} - CN_0(t)N_2(t)$$

$$\frac{dN_1(t)}{dt} = \frac{N_2(t)}{\tau_{21}} - \frac{N_1(t)}{\tau_1} + 2CN_0(t)N_2(t) + C_1^*N_0(t)n_1(t)$$

$$- C_1N_1(t)n_0(t) + q_1'N_0(t)n_2(t) - q_1N_1(t)n_1(t)$$

$$\frac{dN_0(t)}{dt} = -W_p(t)N_0(t) + \frac{N_2(t)}{\tau_{20}} + \frac{N_1(t)}{\tau_1} - CN_0(t)N_2(t)$$

$$+ C_1N_1(t)n_0(t) - C_1^*N_0(t)n_1(t) + q_1N_1(t)n_1(t) - q_1'N_0(t)n_2(t)$$

$$\frac{dn_2(t)}{dt} = q_1N_1(t)n_1(t) - \frac{n_2(t)}{\tau_2'} - q_1'N_0(t)n_2(t)$$

$$\frac{dn_1(t)}{dt} = \frac{n_2(t)}{\tau_{21}'} - \frac{n_1(t)}{\tau_1'} + C_1N_1(t)n_0(t) - C_1^*N_0(t)n_1(t)$$

$$+ q'_1 N_0(t) n_2(t) - q_1 N_1(t) n_1(t) - \sigma v \phi(t) \left(n_1(t) - \frac{g_1}{g_0} n_0(t) \right)$$

$$\begin{aligned} \frac{dn_0(t)}{dt} = & \frac{n_2(t)}{\tau'_{20}} + \frac{n_1(t)}{\tau'_1} + C_1^* N_0(t) n_1(t) - C_1 N_1(t) n_0(t) \\ & + \sigma v \phi(t) \left(n_1(t) - \frac{g_1}{g_0} n_0(t) \right) \end{aligned} \quad (1)$$

In this system, C, C_1^*, C_1, q_1 , and q'_1 represent the probability of cross relaxation, back transfer, forward transfer, up-conversion, and down-conversion, respectively. All of these processes are depicted in Figure 1. The pumping rate is denoted by $W_p(t)$ and represents the number of photons, per microsecond, available to excite electrons in energy level 0 to energy level 2.

The quantities τ_i, τ'_i $i = 1, 2$ represent the spontaneous emission lifetime of energy level i, i' , respectively. The quantity, $\frac{1}{\tau_{ij}}$, represents the transition rate (due to spontaneous emission) from level i to level j . Similarly, $\frac{1}{\tau'_{ij}}$ represents the spontaneous emission transition rate from level i' to level j' . These two quantities satisfy the relations

$$\frac{1}{\tau_i} = \sum_{j=0}^{i-1} \frac{1}{\tau_{ij}} \quad \text{and} \quad \frac{1}{\tau'_i} = \sum_{j=0}^{i-1} \frac{1}{\tau'_{ij}} \quad i = 1, 2$$

The photon density is denoted by $\phi(t)$ and the rate equation describing the temporal evolution of the photon density in the optical cavity is given by

$$\frac{d\phi(t)}{dt} = v \sigma \phi(t) \left(n_1(t) - \frac{g_1}{g_0} n_0(t) \right) - \frac{\phi(t)}{\tau_c} + s p_o \frac{n_1(t)}{\tau_{f1}}. \quad (2)$$

Here, σ denotes the transition cross section, v is the velocity of light in the laser crystal, g_1 is the number of manifolds associated with energy level $1'$ and likewise

for g_0 . The contribution due to spontaneous emission of holmium ions in energy level 1' is denoted sp_0 and the fluorescent lifetime of the material is denoted τ_{fl} . The lifetime of a photon in the optical cavity is denoted by τ_c and can be expressed as [2]

$$\tau_c = \frac{2\ell_c/c}{-\ln R_1 R_2},$$

where ℓ_c is the length of the optical cavity, c is the velocity of light *in vacuo* and R_1 & R_2 denote the reflectivity of the two mirrors. The electron populations of thulium and holmium are constrained by the relations

$$N_T = N_0(t) + N_1(t) + N_2(t) \quad \text{and} \quad n_T = n_0(t) + n_1(t) + n_2(t) \quad (3)$$

where N_T is the concentration of thulium ions, per cm^3 , and n_T is the concentration of holmium ions, per cm^3 .

These "population constraints" can be rewritten as

$$N_0(t) = N_T - N_1(t) - N_2(t) \quad \text{and} \quad n_0(t) = n_T - n_1(t) - n_2(t) \quad (4)$$

Substituting these expressions for $N_0(t)$ and $n_0(t)$ into system (1) reduces the system from six to four equations. Then by including the rate equation for the photon density (2) we obtain

$$\frac{dN_2(t)}{dt} = W_p(t)(N_T - N_1(t) - N_2(t)) - \frac{N_2(t)}{\tau_2} - CN_2(t)(N_T - N_1(t) - N_2(t))$$

$$\frac{dN_1(t)}{dt} = \frac{N_2(t)}{\tau_{21}} - \frac{N_1(t)}{\tau_1} + 2CN_2(t)(N_T - N_1(t) - N_2(t))$$

$$+ C_1^* n_1(t)(N_T - N_1(t) - N_2(t)) - C_1 N_1(t)(n_T - n_1(t) - n_2(t))$$

$$+ q_1' n_2(t)(N_T - N_1(t) - N_2(t)) - q_1 N_1(t) n_1(t)$$

$$\frac{dn_2(t)}{dt} = q_1 N_1(t) n_1(t) - \frac{n_2(t)}{\tau_2'} - q_1' n_2(t)(N_T - N_1(t) - N_2(t))$$

$$\frac{dn_1(t)}{dt} = \frac{n_2(t)}{\tau_{21}'} - \frac{n_1(t)}{\tau_1'} + C_1 N_1(t)(n_T - n_1(t) - n_2(t))$$

$$- C_1^* n_1(t)(N_T - N_1(t) - N_2(t)) + q_1' n_2(t)(N_T - N_1(t) - N_2(t))$$

$$- q_1 N_1(t) n_1(t) - \sigma v \phi(t) \left(n_1(t) - \frac{g_1}{g_0} (n_T - n_1(t) - n_2(t)) \right)$$

$$\frac{d\phi(t)}{dt} = v \sigma \phi(t) \left(n_1(t) - \frac{g_1}{g_0} n_0(t) \right) - \frac{\phi(t)}{\tau_c} + s p_o \frac{n_1(t)}{\tau_{fl}} \quad (5)$$

The coupled system (5) is the temporal model of the laser system expressed in terms of the physical variables. We now normalize system (5) to put it into the form used for the analysis and calculations of the subsequent sections. Hence, let

$$x(t) = \frac{N_2(t)}{N_T}$$

$$y(t) = \frac{N_1(t)}{N_T}$$

$$z(t) = \frac{n_1(t)}{n_T}$$

$$w(t) = \frac{n_2(t)}{n_T}$$

$$P(t) = \frac{\phi(t)}{\phi_{norm}} \quad (6)$$

be the normalized variables. Rewriting the rate equations (5) in terms of the normalized variables (6) yields

$$\frac{dx}{dt} = W_p(t)(1 - x - y) - \frac{x}{\tau_2} - D_1 x(1 - x - y)$$

$$\frac{dy}{dt} = \frac{x}{\tau_{21}} - \frac{y}{\tau_1} + 2D_1 x(1 - x - y) + D_3 z(1 - x - y)$$

$$- D_2 y(1 - z - w) + D_6 w(1 - x - y) - D_7 yz$$

$$\frac{dw}{dt} = D_8 yz - \frac{w}{\tau'_2} - D_9 w(1 - x - y)$$

$$\frac{dz}{dt} = \frac{w}{\tau'_{21}} - \frac{z}{\tau'_1} + D_4 y(1 - z - w) - D_5 z(1 - x - y)$$

$$+ D_9 w(1 - x - y) - D_8 yz - \beta_1[\gamma z + (1 - \gamma)(1 - w)]P$$

$$\frac{dP}{dt} = \left\{ \beta_2 [\gamma z + (1 - \gamma)(1 - w)] - \frac{1}{\tau_c} \right\} P + \beta_3 z \quad (7)$$

where

$$D_1 = CN_T \quad D_4 = C_1 N_T \quad D_7 = q_1 n_T \quad \beta_1 = \sigma v \phi_{\text{norm}}$$

$$D_2 = C_1 n_T \quad D_5 = C_1^* N_T \quad D_8 = q_1 N_T \quad \beta_2 = \sigma v n_T$$

$$D_3 = C_1^* n_T \quad D_6 = q_1' n_T \quad D_9 = q_1' N_T \quad \beta_3 = \frac{sp_o n_T}{\tau_{fl} \phi_{\text{norm}}}$$

$$\gamma = 1 + \frac{g_1}{g_0}$$

Qualitative Analysis

In this section the full set of equations, (7), is modified by excluding two physical processes—up-conversion and back transfer. This yields a simplified system for which certain qualitative properties of the solution are established. Throughout this discussion, the parameters are assumed to satisfy the following (physically realistic) relationships :

$$\tau_{21} > \tau_2 > 0$$

$$\tau_1 > \tau_{20} > 0$$

$$\tau_1' > \tau_c > 0$$

$$\beta_1, \beta_2, \beta_3 > 0$$

$$D_1, D_2, D_4 > 0$$

$$1 < \gamma$$

$$sp_o \ll 1$$

Excluding the above mentioned processes yields the following simplified system of rate equations

$$\frac{dx}{dt} = W_p(t)(1-x-y)_+ - \frac{x}{\tau_2} - D_1x(1-x-y)_+$$

$$\frac{dy}{dt} = \frac{x}{\tau_{21}} - \frac{y}{\tau_1} + 2D_1x(1-x-y)_+ - D_2y(1-z)_+$$

$$\frac{dz}{dt} = -\frac{z}{\tau'_1} + D_4y(1-z)_+ + \beta_1(\gamma(1-z)_+ - 1)P$$

$$\frac{dP}{dt} = \left\{ \beta_2[1 - \gamma(1-z)_+] - \frac{1}{\tau_c} \right\} P + \beta_3z$$

(8)

where

$$(1-x-y)_+ = \begin{cases} 1-x-y & \text{if } 1-x-y \geq 0 \\ 0 & \text{otherwise} \end{cases}$$

$$(1-z)_+ = \begin{cases} 1-z & \text{if } 1-z \geq 0 \\ 0 & \text{otherwise} \end{cases}$$

(9)

The system of equations (8) can be written symbolically as

$$y' = f(t, y)$$

where

$$y = \begin{bmatrix} x \\ y \\ z \\ P \end{bmatrix} \quad \text{and} \quad f(t, y) = \begin{bmatrix} W_p(t)(1 - x - y)_+ - \frac{x}{\tau_2} - D_1 x(1 - x - y)_+ \\ \frac{x}{\tau_{21}} - \frac{y}{\tau_1} + 2D_1 x(1 - x - y)_+ - D_2 y(1 - z)_+ \\ -\frac{z}{\tau_1'} + D_4 y(1 - z)_+ + \beta_1(\gamma(1 - z)_+ - 1)P \\ \left\{ \beta_2[1 - \gamma(1 - z)_+] - \frac{1}{\tau_c} \right\} P + \beta_3 z \end{bmatrix}$$

It now follows directly from [3] that if (i) $W_p(t)$ is continuous and (ii) the solution vector, y , is bounded then there exists a unique, continuous solution to the system (8). The following four theorems may be viewed as a validation of the model since they show that the solution to the system (8) possesses the same qualitative properties that one would expect the laser system to possess. The proofs of the theorems can be found in [4]. The first theorem establishes the nonnegativity of the solution vector y , as well as the ground states of thulium and holmium.

Theorem 1 (Nonnegativity) *If $W_p(t) > 0$ for $t > 0$ and $x(0) \geq 0$, $y(0) \geq 0$, $z(0) \geq 0$, and $P(0) \geq 0$ then*

(i) *If $1 - x(0) - y(0) > 0$ then $1 - x(t) - y(t) > 0$ for all $t > 0$;*

(ii) *If $1 - x(0) - y(0) < 0$ then there exists a T such that $1 - x(t) - y(t) > 0$ for all $t > T$;*

- (iii) (a) If $1 - x(0) - y(0) > 0$ then $x(t) > 0$ and $y(t) > 0$ for all $t > 0$
- (b) If $1 - x(0) - y(0) \leq 0$ then $x(t) \geq 0$ and $y(t) > 0$ for all $t > 0$;
- (iv) If $1 - z(0) > 0$ then $1 - z(t) > 0$ for all $t > 0$;
- (v) If $1 - z(0) < 0$ then there exists a T^* such that $1 - z(t) > 0$ for all $t > T^*$;
- (vi) $z(t) > 0$ and $P(t) > 0$ for all $t > 0$.

Theorem 1 states that the normalized ground levels of thulium and holmium remain nonnegative on $\mathcal{I} = [0, \infty)$ or in other words that the constraints (9) are self-enforcing. Consequently, we will drop the “+” subscripts in system (8) for the remainder of the discussion.

Theorem 2 (Integrability) *Let $W_p(t)$ be positive, continuous, and integrable on \mathcal{I} . Then if $x(0) \geq 0$, $y(0) \geq 0$, $z(0) \geq 0$, & $P(0) \geq 0$, then $x(t)$, $y(t)$, $z(t)$, & $P(t)$ are all integrable on \mathcal{I} .*

Theorem 3 (Boundedness) *If $W_p(t) > 0$ on \mathcal{I} then $x(t)$, $y(t)$, $z(t)$, and $P(t)$ are all bounded on \mathcal{I} .*

Finally, Theorem 4 gives the behaviour of the solution when the pumping term $W_p(t)$ decays to zero but doesn't decay quickly enough to be integrable on $[0, \infty)$.

Theorem 4 *Let W_p , x , y , z , and P satisfy the hypotheses of Theorem 1. Furthermore, let $W_p(t) \rightarrow 0$ as $t \rightarrow \infty$. Then, the solution vector $\mathbf{y} \rightarrow 0$ as $t \rightarrow \infty$.*

Stability Analysis

In this section the equilibrium solutions are obtained and a local stability analysis is performed. Before doing this however we make the simplifying assumption that the spontaneous emission term, sp_o , has a negligible affect on the asymptotic behaviour of the system and hence may be dropped. Furthermore, we will consider the case of continuous wave (CW) pumping. These two considerations are tantamount to taking $\beta_3 \equiv 0$ and $W_p(t) \equiv W_p$ in system (8), where W_p is a positive constant. Doing this yields the following system of rate equations :

$$\begin{aligned} \frac{dx}{dt} &= W_p(1 - x - y) - \frac{x}{\tau_2} - D_1x(1 - x - y) \\ \frac{dy}{dt} &= \frac{x}{\tau_{21}} - \frac{y}{\tau_1} + 2D_1x(1 - x - y) - D_2y(1 - z) \\ \frac{dz}{dt} &= -\frac{z}{\tau_1} + D_4y(1 - z) + \beta_1[\gamma(1 - z) - 1]P \\ \frac{dP}{dt} &= \left\{ \beta_2[1 - \gamma(1 - z)] - \frac{1}{\tau_c} \right\} P \end{aligned} \tag{10}$$

By setting the right hand side of equations (10) equal to zero, two equilibrium points are obtained. Equilibrium point 1, denoted **I**, which has coordinates $(x^1, y^1, z^1, 0)$ and equilibrium point 2, denoted **II**, which has coordinates (x^2, y^2, z^2, P^2) , where the coordinates are expressed in terms of the physical parameters of the system and are given in [5].

Having located the equilibrium points we now determine the stability properties of I and II. For the stability of I, introduce the new hat variables given by $\hat{x} = x - x^1$, $\hat{y} = y - y^1$, $\hat{z} = z - z^1$, and $\hat{P} = P - 0$. Substituting these variables into the system of rate equations (10) yields

$$\begin{aligned} \frac{d\hat{x}}{dt} = & \left(D_1 x^1 - W_p - \frac{1}{\tau_2} - D_1(1 - x^1 - y^1) \right) \hat{x} \\ & + (D_1 x^1 - W_p) \hat{y} + \underbrace{D_1(\hat{x})^2 + D_1 \hat{x} \hat{y}}_{\hat{g}_1} \end{aligned}$$

$$\begin{aligned} \frac{d\hat{y}}{dt} = & \left(\frac{1}{\tau_{21}} + 2D_1(1 - x^1 - y^1) - 2D_1 x^1 \right) \hat{x} \\ & - \left(\frac{1}{\tau_1} + 2D_1 x^1 + D_2(1 - z^1) \right) \hat{y} + D_2 y^1 \hat{z} \\ & + \underbrace{D_2 \hat{y} \hat{z} - 2D_1(\hat{x})^2 - 2D_1 \hat{x} \hat{y}}_{\hat{g}_2} \end{aligned}$$

$$\begin{aligned} \frac{d\hat{z}}{dt} = & (D_4 - D_4 z^1) \hat{y} + \left(-\frac{1}{\tau_1} - D_4 y^1 \right) \hat{z} \\ & + \beta_1(\gamma - \gamma z^1 - 1) \hat{P} + \underbrace{-D_4 \hat{y} \hat{z} - \gamma \beta_1 \hat{z} \hat{P}}_{\hat{g}_3} \end{aligned}$$

$$\frac{d\hat{P}}{dt} = \left\{ \beta_2(1 - \gamma + \gamma z^1) - \frac{1}{\tau_c} \right\} \hat{P} + \underbrace{\beta_2 \gamma \hat{z} \hat{P}}_{\hat{g}_4}$$

Now, letting $\hat{X} = [\hat{x}, \hat{y}, \hat{z}, \hat{P}]^T$ & $\hat{g} = [\hat{g}_1, \hat{g}_2, \hat{g}_3, \hat{g}_4]^T$, the above system may be written more compactly as

$$\dot{\hat{X}} = \hat{A}\hat{X} + \hat{g} \quad (11)$$

where \hat{A} represents the coefficient matrix of the associated linear system. This is an "almost linear" system so I will be asymptotically stable if the eigenvalues of \hat{A}

have negative real parts. Invoking the Routh-Hurwitz Theorem [6] the following necessary and sufficient condition for **I** to be asymptotically stable is obtained

$$\beta_2[1 - \gamma(1 - z^1)] - \frac{1}{\tau_c} < 0$$

The stability analysis for **II** parallels that of **I** and yields one condition for **II** to be asymptotically stable. The algebra associated with this condition, however, is tremendously complicated and hence we resort to a parametric investigation of the stability of the equilibrium points.

The numerics indicate there is an interplay of stability between **I** and **II**. To see this, consider W_p as a parameter and choose it to be "small". By computing the equilibrium values of **I** & **II** and then checking the Routh-Hurwitz Criteria, the stability of each point is determined. By gradually increasing W_p and repeating the process we see there is an interchange of stability that goes like this. For W_p small, the P coordinate of **II** is negative, **II** is unstable, and **I** is asymptotically stable (i.e. no lasing). As W_p is increased, the P coordinate of **II** eventually reaches zero and thus the two equilibrium points coalesce (this is the threshold of lasing). Finally, as W_p is increased still further, the P coordinate of **II** becomes positive, **II** becomes asymptotically stable, and **I** becomes unstable (i.e. lasing occurs).

This is illustrated in Figure 2 where P^2 is graphed as a function of W_p and the stability of **I** and **II** is noted. The value of W_p at which the interchange of stability occurs is a bifurcation point and is denoted W_p^* . From numerical calculations it was found that $W_p^* \doteq 0.342 \times 10^{-5}$.

It is also of physical interest to see how the system responds as the cavity lifetime of a photon, τ_c , is varied. Choosing τ_c small and following the same procedure as above yields the same interplay of stability as before. Figure 3 gives P^2 as a function of τ_c , once again noting the stability of each point. From this we see that τ_c has a bifurcation point which will be denoted τ_c^* and is approximated by $\tau_c^* \doteq 4.81 \times 10^{-5}$. Insert Figures 2 & 3

Numerical Analysis

In this section the numerical solution to system (8) is obtained. This is done by employing either the subroutine LSODA (when using a VAX 11/750) or the subroutine DDRIV2 (when using an IBM PC). In either case, all computations were performed in double precision arithmetic. LSODA was developed in 1987 at Lawrence Livermore National Laboratory in Livermore, California by L.R. Petzold and A.C. Hindmarsh. DDRIV2 was developed in 1979 and revised in 1987 by D.K. Kahaner, National Bureau of Standards, and C.D. Sutherland of Los Alamos National Laboratory. Both subroutines were created for the numerical integration of stiff and nonstiff systems of first order ordinary differential equations. When the system is stiff, the subroutines use a backward difference formula (BDF) to perform the numerical integration and when the system is not stiff they use a higher order Adams method. Both LSODA and DDRIV2 have the capability of automatically switching from one method to the other as the system passes from stiff to nonstiff regions. The BDF method was chosen by both d.e. solvers throughout the interval of integration which indicates that system

(8) is stiff. Roughly speaking, a system is stiff when the characteristic equation of the associated linear system has a root with a “large” negative real part. A more detailed treatment of stiffness can be found in [7]. The numerical values of the system parameters are given in Table 1 and were used in the computation of the numerical solution. Insert Table 1 Employing the program in [8] the numerical solution of (8) was obtained. A typical example of the numerical solution is given in Figure 4 where the upper lasing level and the photon density are plotted. Insert Figure 4 Since W_p is constant, a comparison of the “long time” behaviour of the numerical solutions with that of the equilibrium solutions can be performed. Using the parameter values in Table 1 and the Routh-Hurwitz criteria for asymptotic stability it is found that **II** is asymptotically stable and **I** is unstable. The coordinates of **II**, as predicted by the stability analysis are given in the left column below and the numerical solutions at $t = 200\mu s$ are given in the right column below.

$$x^2 = 0.1304363 \quad x = 0.1304372$$

$$y^2 = 0.7637408 \quad y = 0.7637406$$

$$z^2 = 0.5238095 \quad z = 0.5238095$$

$$P^2 = 0.0759492 \quad P = 0.0759491$$

From this it is evident that the d.e. solver captures the “long time” behaviour of the solutions extremely well.

Various pumping schemes were considered in the model. Figure 5 gives the

numerical solution for $P(t)$ when the pump term is taken to be

$$W_p(t) = \alpha^2 t e^{-\alpha^2 t^2}$$

where $\alpha = .01133$. From this figure we see that the photon density has irregular oscillations and decays rather rapidly, becoming negligible by about $t = 250\mu s$.

Insert Figure 5

We now consider two modifications that are made to upgrade the model. The first is to include the terms that account for the back transfer of energy and that were excluded at the beginning of the section on qualitative analysis. The second is to replace β_2 & β_3 in the rate equation for the photon density with

$$\beta'_2 = \left(\frac{\ell}{\ell_c}\right) \beta_2 \quad \& \quad \beta'_3 = \left(\frac{\ell}{\ell_c}\right) \beta_3.$$

The rationale for the second change is as follows. A mathematical model that accurately describes the dynamics of a laser system must account for both spatial and temporal variations in the dependent variables. Allowing for both types of variation yields a system of nonlinear partial differential equations (p.d.e.'s). Due to the intractability of the equations and the amount of effort and computer time involved in solving the system numerically, various averaging techniques are used to eliminate the spatial dependence and thus make the system more tractable. L.F. Roberts et.al. [9] gives three such averaging schemes along with their resultant o.d.e. models. The conclusion of this work is that only the temporal model obtained by taking a spatial average over the optical length of the cavity, ℓ_c , yields numerical results that agree qualitatively with those predicted by the spatial and

temporal model. This averaging scheme can be incorporated into the model by replacing β_2 and β_3 by the quantities given above. Doing this and including the back transfer terms yields the system

$$\begin{aligned}
\frac{dx}{dt} &= W_p(t)(1 - x - y) - \frac{x}{\tau_2} - D_1x(1 - x - y) \\
\frac{dy}{dt} &= \frac{x}{\tau_{21}} - \frac{y}{\tau_1} + 2D_1x(1 - x - y) - D_2y(1 - z) + D_3z(1 - x - y) \\
\frac{dz}{dt} &= -\frac{z}{\tau_1} + D_4y(1 - z) - D_5z(1 - x - y) + \beta_1[\gamma(1 - z) - 1]P \\
\frac{dP}{dt} &= \left\{ \beta'_2[1 - \gamma(1 - z)] - \frac{1}{\tau_c} \right\} P + \beta'_3z
\end{aligned} \tag{12}$$

The numerical solution to the system (12) was obtained giving special attention to the qualitative behaviour of the photon density for various values of C_1^* and $\frac{\ell}{\ell_c}$. Recall that C_1^* represents the probability of back transfer occurring. The pumping term was taken to be of the form

$$W_p(t) = \alpha^2 t e^{-\alpha^2 t^2}.$$

In Figure 6 the normalized photon density is graphed for a set of parameter values that are "close" to the values used in experimentation. Comparing Figure 6 with Figure 5 we see a salient disparity in the qualitative behaviour of the photon density. The previously observed erratic spiking has been replaced by regular and temperate oscillations. Figure 7 is a picture of the energy output of the laser

system as displayed on the screen of an oscilloscope.

Insert Figures 6 & 7

By comparing Figure 6 with Figure 7 we see that the behaviour of the photon density, as predicted by the temporal model (12), is in remarkable agreement with the behaviour observed in the laboratory (both having about 7 oscillations in 25 μs).

Finally, we further upgrade the model by including the terms associated with the up-conversion of energy from the 5I_7 energy level to the 5I_5 energy level of holmium. This now brings us full circle since we are back to the full set of equations (7) with the exception that β_2 & β_3 are replaced by β'_2 & β'_3 , respectively, as defined above. The numerical solution to the system with up-conversion was computed taking the probability of up-conversion & down-conversion as

$$q_1 = 5.0 \times 10^{-22} \quad \& \quad q'_1 = 1.2 \times 10^{-23}$$

respectively. Figure 8 shows the interplay between the photon density and the upper lasing level of holmium and Figure 9 gives a phase portrait of the same.

Insert Figures 8 & 9

Summary and Conclusions

We have developed a temporal model of the dynamics of an optically pumped co-doped six-level solid state laser. The model was developed to study the inter-ionic transfer of energy between thulium and holmium and how this affects the performance of the laser system. In this paper we report on the quantitative and qualitative behaviour of the solutions.

The validity of the simplified model was established by showing that— under appropriate conditions on the pumping term— solutions to the system exist and are bounded. Further, we showed that if the initial conditions are physically realistic and the pumping term is well enough behaved, then the solutions are both nonnegative and integrable (integrability is desirable since calculating the efficiency of the laser system involves integrating over the photon density).

Two equilibrium solutions were obtained and a local stability analysis performed. The interplay of stability between the two equilibrium points was then demonstrated parametrically.

The system was solved numerically and found to be stiff. The d.e. solvers used performed exceptionally well and gave numerical solutions that agreed with the stability analysis and the experimental results. By gradually upgrading the simplified model it was found that both back transfer and up-conversion affect the time of lasing as well as the magnitude and frequency of the laser output but it is an alternate averaging scheme that has the most dramatic affect on the qualitative behaviour of the output pulse.

Acknowledgements

This work was supported by N.A.S.A./Langley Research Center. The project was overseen by Dr. Clay Bair, Dr. Phil Brockman and Dr. Bob Hess, in the Laser Technology and Applications Branch of F.E.D. T.G. Wangler was supported by N.A.S.A. grant NGT-50346; J.J. Swetits was supported by N.A.S.A. grant NAG-1- 957, and A.M. Buoncristiani was supported by N.A.S.A. grant NAG-1-796.

1. T.G. Wangler, "Ph.D. Dissertation", Old Dominion University, Figure 2.1, p.10
2. O. Svelto, *Principles of Lasers*, Plenum Press, 1989
3. F. Brauer and J.A. Nohel, *Qualitative Theory of Ordinary Differential Equations*, W.A. Benjamin Inc., 1969, p.26
4. T.G. Wangler, "Ph.D. Dissertation", Old Dominion University, pp.48-68
5. T.G. Wangler, "Ph.D. Dissertation", Old Dominion University, pp.71-73
6. D.A. Sanchez, *Ordinary Differential Equations and Stability Theory: An Introduction*, Dover, 1979, p.57
7. D. Kahaner, C. Moler and S. Nash, *Numerical Methods and Software*, Prentice Hall, 1989, pp.284 ff.
8. T.G. Wangler, "Ph.D. Dissertation", Old Dominion University, Appendix B
9. L.F. Roberts, A.M. Buoncristiani and J.J. Swetits, "An Investigation of a Mathematical Model of the Dynamics of an End-Pumped $Ti : Al_2O_3$ Laser System", (Pending Publication)

Table 1 System Parameters for Tm-Ho:YAG Laser

$$N_T = 1 \times 10^{21}/cm^3$$

$$n_T = 1 \times 10^{20}/cm^3$$

$$\ell = 0.3 \text{ cm}$$

$$\phi_{norm} = 1 \times 10^{18}/cm^3$$

$$\ell_c = 17.5 \text{ cm}$$

$$R_1 = 1.0$$

$$R_2 = 0.95$$

$$C = \frac{1}{40 \times 10^{21}} \text{ cm}^3/\mu s$$

$$C_1 = \frac{1}{475 \times 10^{20}} \text{ cm}^3/\mu s$$

$$C_1^* = 0.0$$

$$\tau_2 = 450 \mu s$$

$$\tau_{20} = 900 \mu s$$

$$\tau_{21} = 900 \mu s$$

$$\tau_1 = 11,000 \mu s$$

$$\tau_1' = 8,500 \mu s$$

$$g_0 = 1$$

$$g_1 = 1$$

$$\gamma = 2$$

$$\sigma = 7 \times 10^{-21} \text{ cm}^2$$

$$q_1 = 0.0$$

$$q_1' = 0.0$$

$$v = 30,000 \text{ cm}/\mu s$$

$$\tau_c = 1 \times 10^{-3} \mu s$$

$$W_p = 6 \times 10^{-3}/cm^3 \cdot \mu s$$

$$sp_o = 1 \times 10^{-6}$$

Figure 1

Idealized model of the Tm-Ho:YAG laser with the following processes represented: (a) Stimulated Absorption, (b) Cross Relaxation, (c) Back Transfer, (d) Forward Transfer, (e) Up-Conversion, (f) Down-Conversion, and (g) Stimulated Emission.

Figure 2

P coordinate of **II** as a function of the pumping term.

Figure 3

P coordinate of **II** as a function of the cavity lifetime τ_c .

Figure 4

Normalized photon density and upper lasing level with a constant pump.

Figure 5

Normalized photon density with a decaying exponential pump.

Figure 6

Photon density when using an alternate averaging technique.

Figure 7

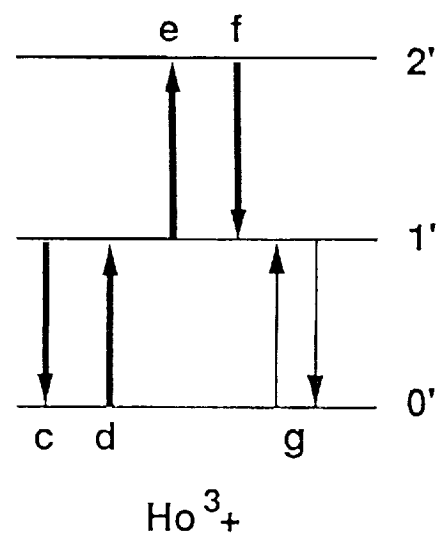
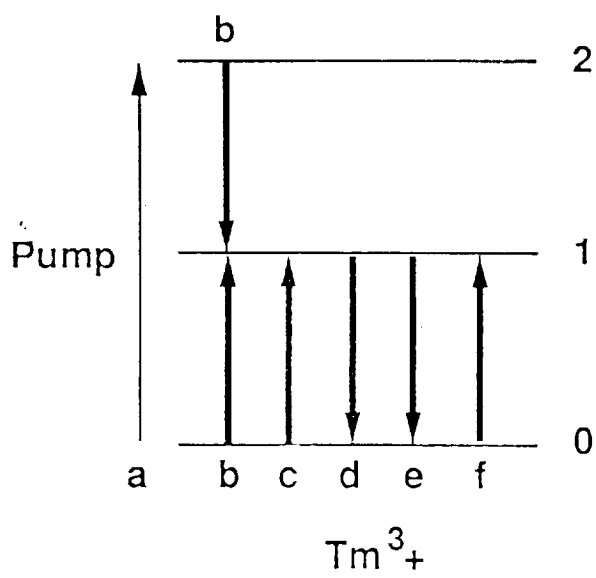
The energy output of the Tm-Ho:YAG laser as displayed on the screen of an oscilloscope.

Figure 8

Upper lasing level and photon density with up-conversion included in the model.

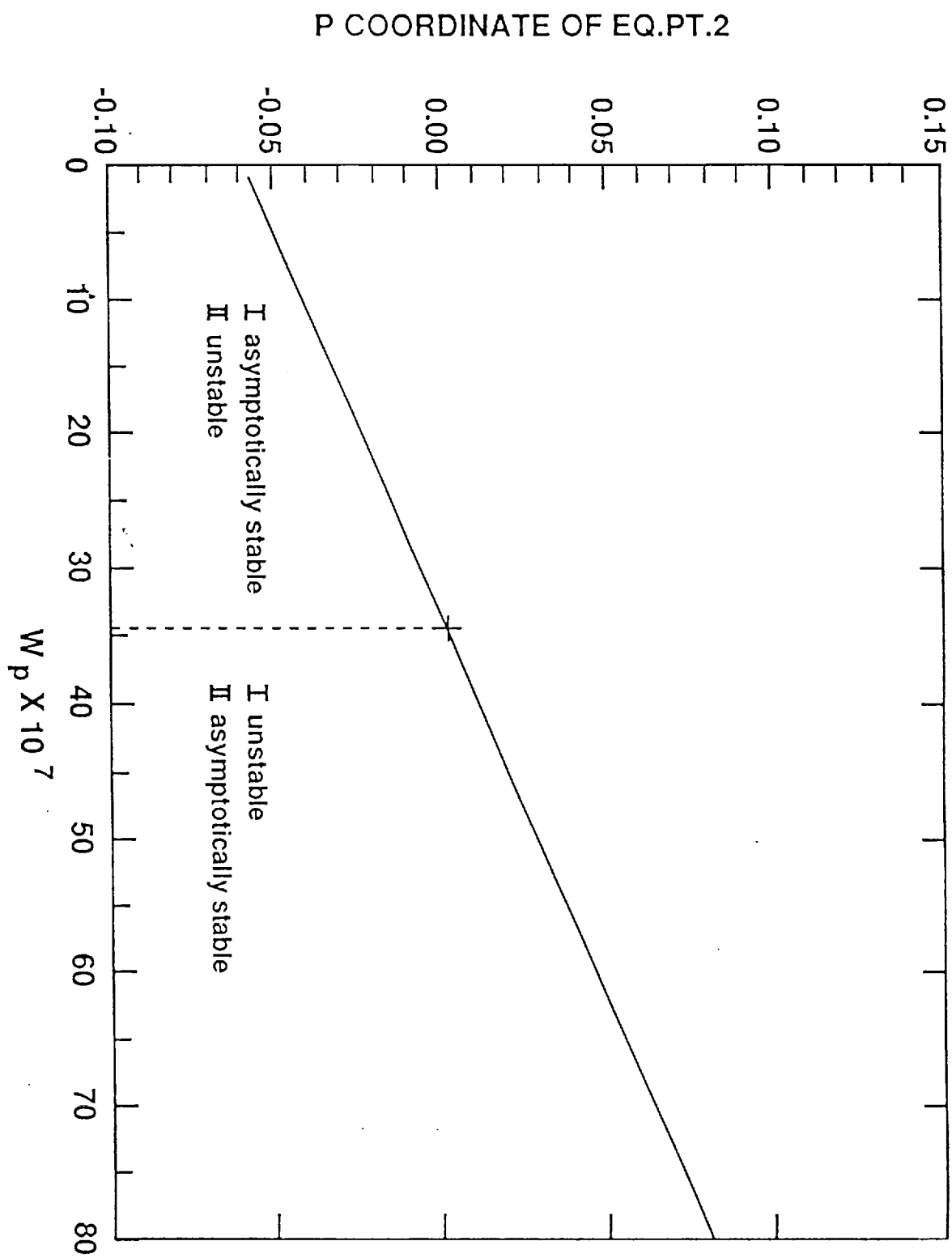
Figure 9

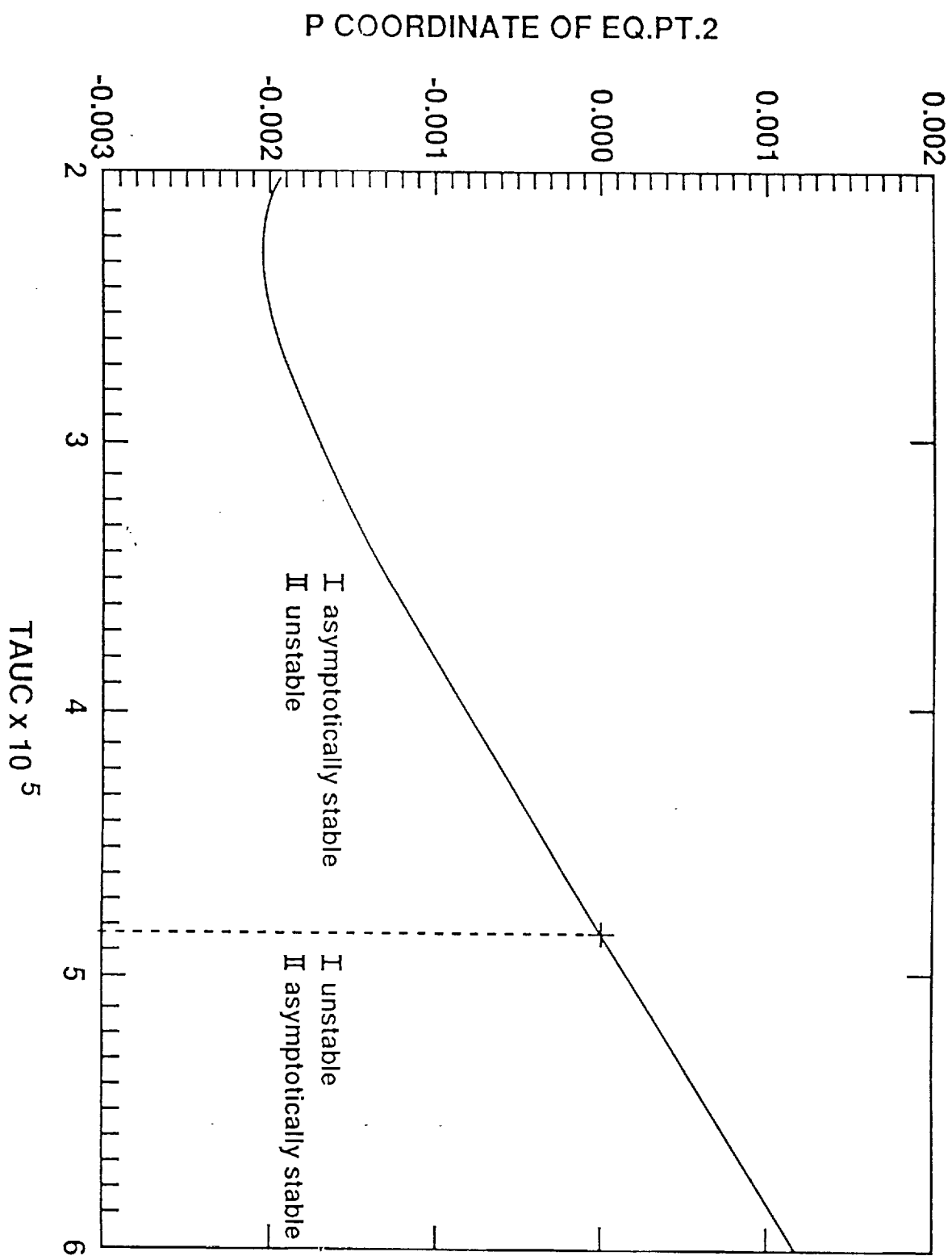
Phase portrait of the upper lasing level and the photon density.

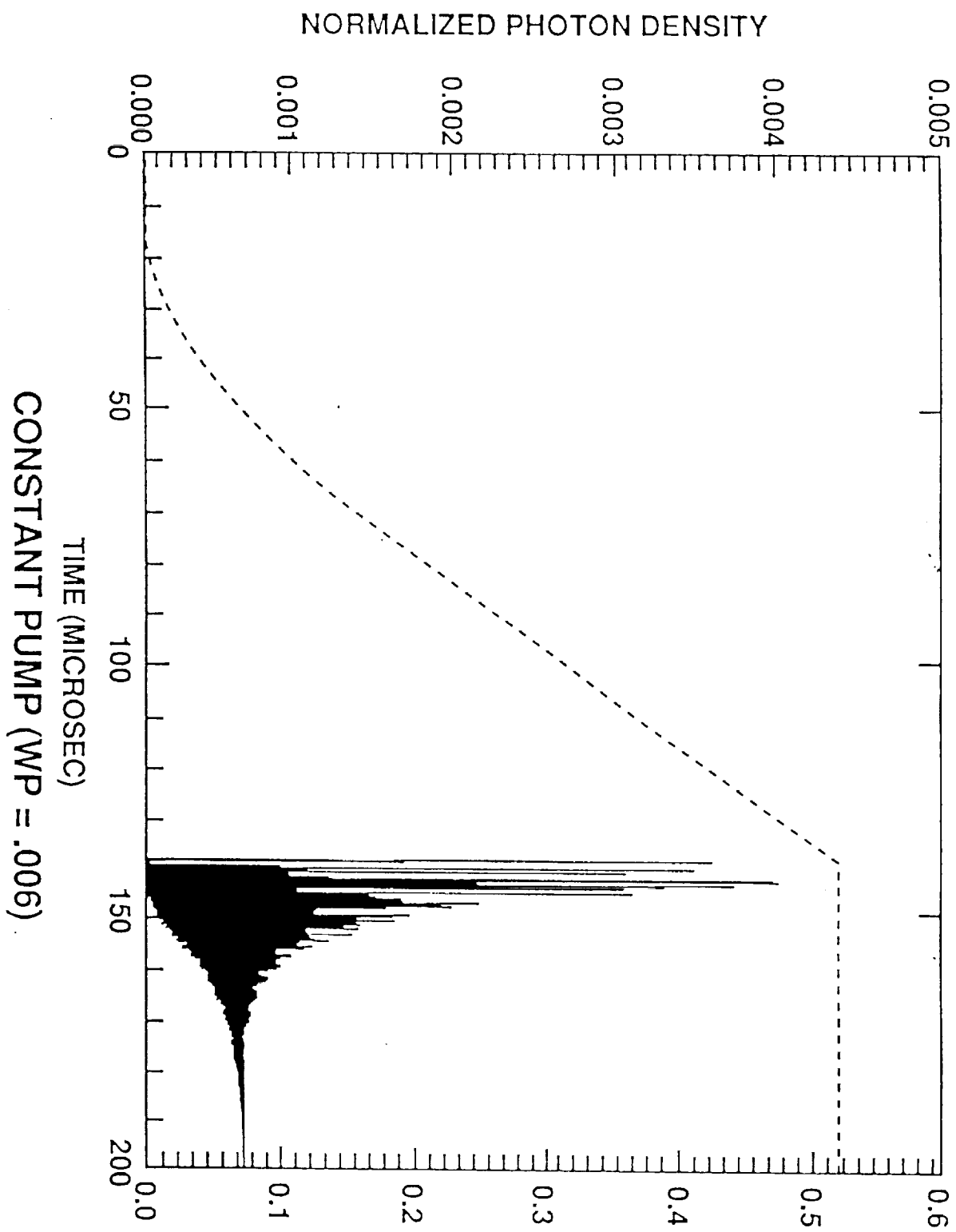


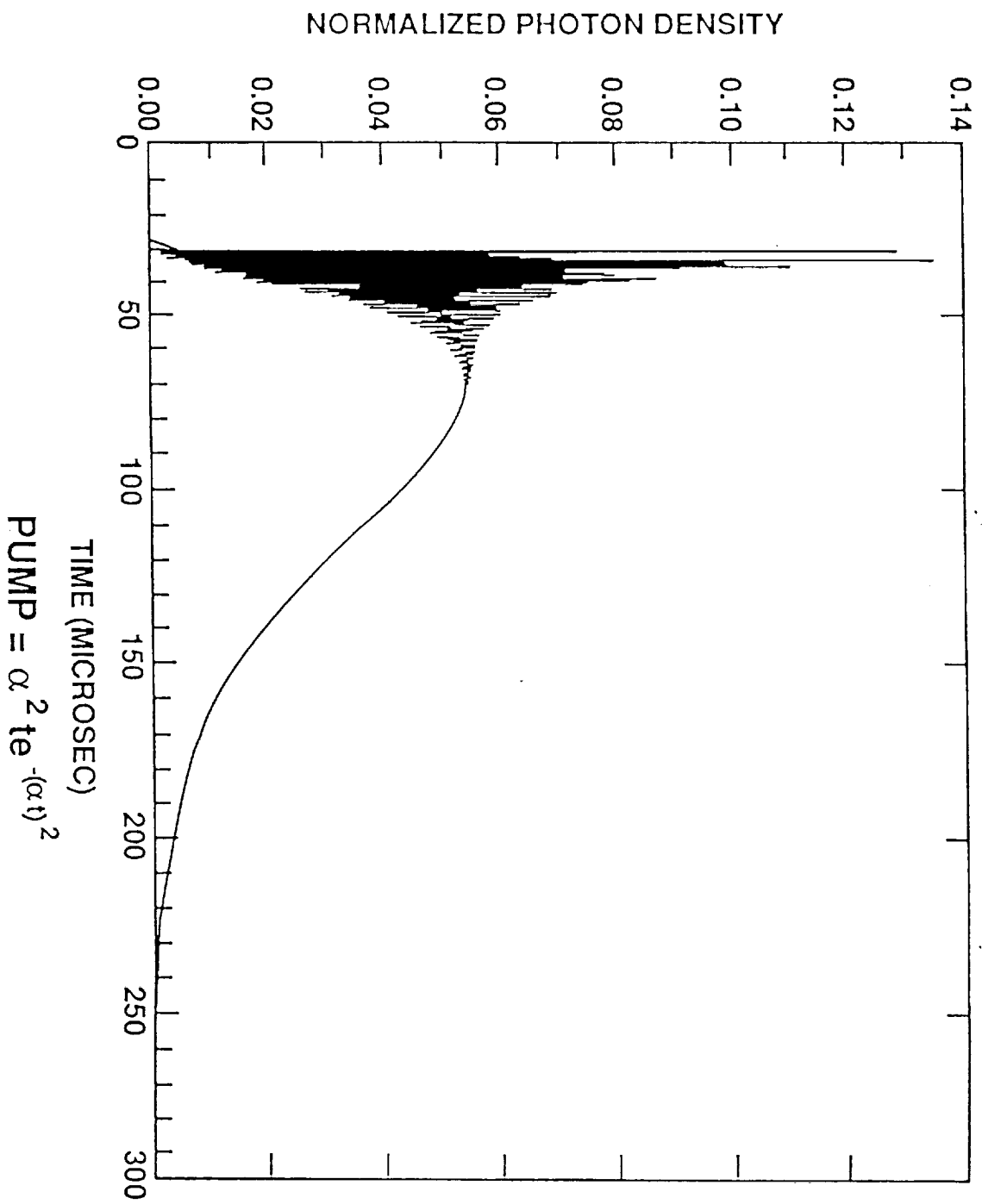
Radiative
Transition

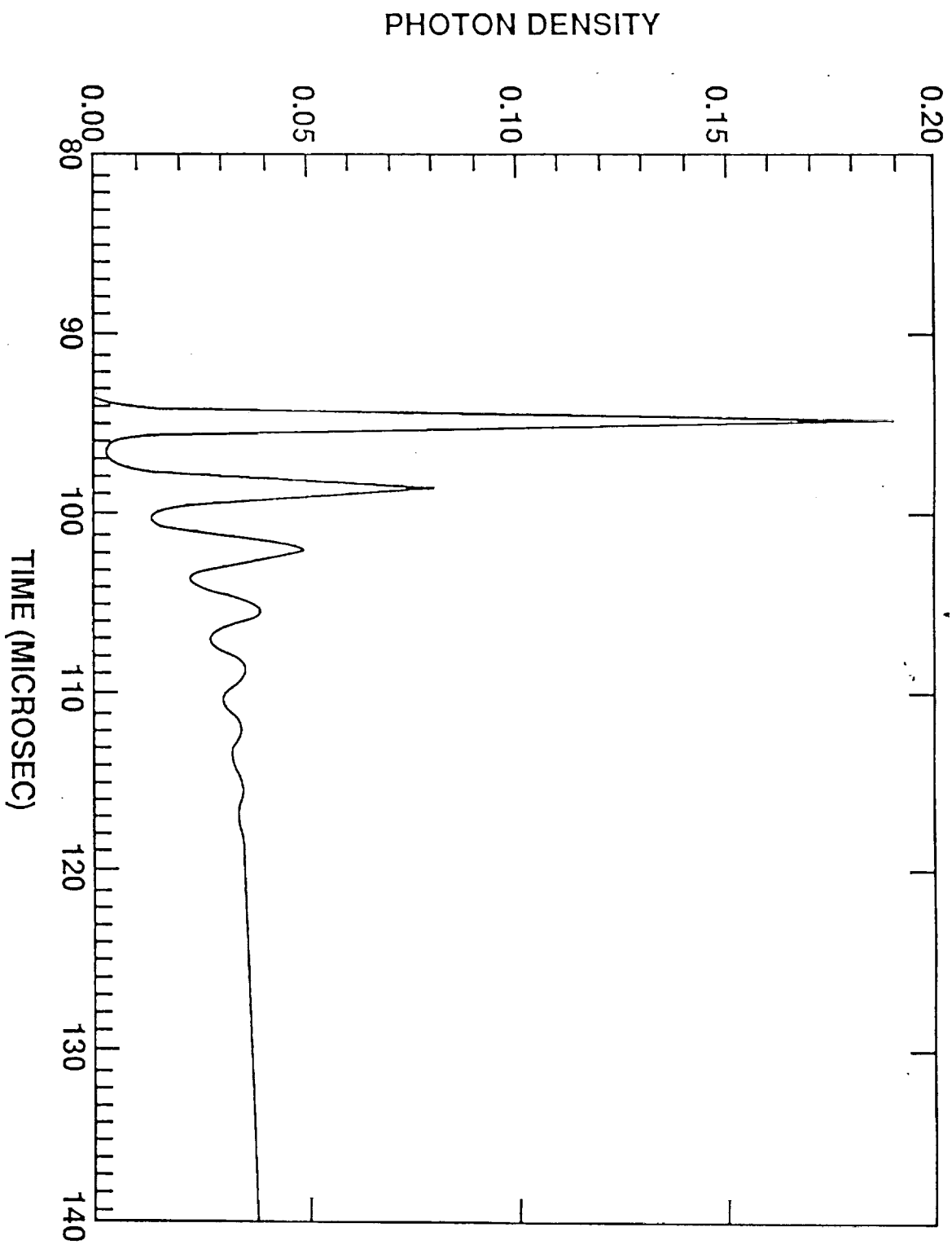
Non-Radiative
Transition











C1STAR = 3.25D - 22 L = 0.3 Lc = 17.5 Q1 = 0

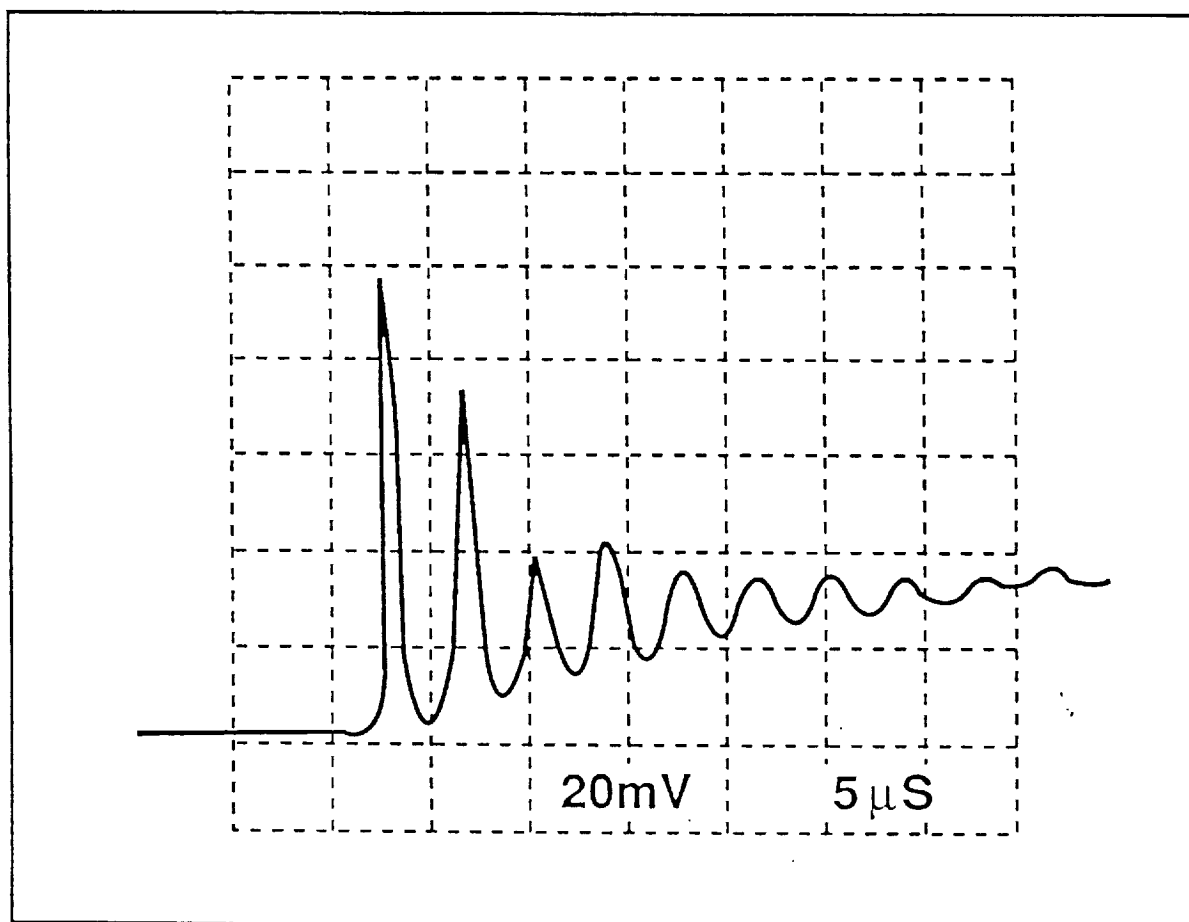


Fig. 7

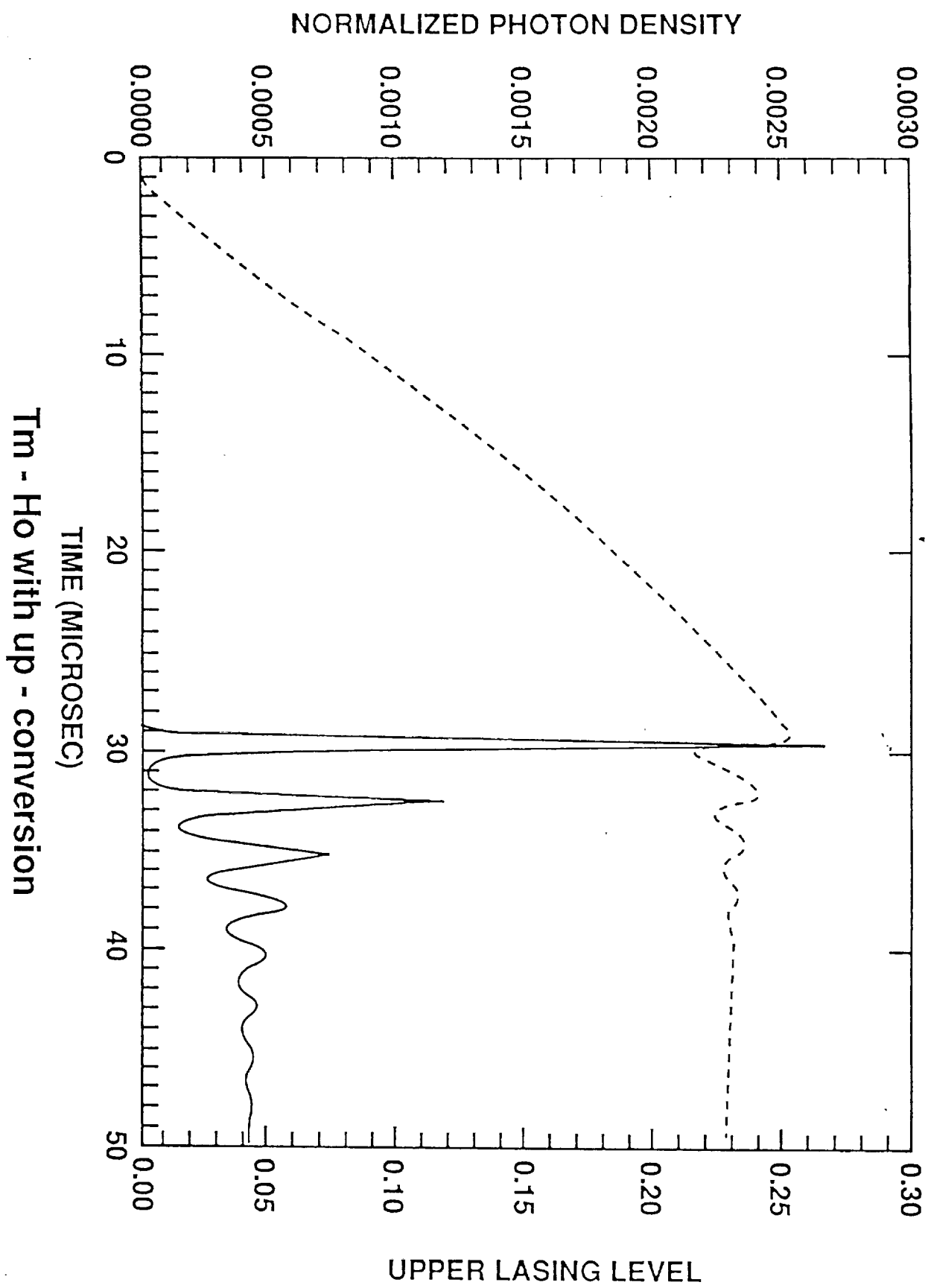


Fig. 8

